

Initial Rotor Position Detection of Induction Machines Using Feedforward Sensorless Saliency Separation

Research paper

Eduardo Rodriguez Montero^{1,*}, Markus Vogelsberger², Thomas Wolbank¹

¹Institute of Energy Systems and Electrical Drives, Technische Universität Wien, Vienna, Austria

²Rolling Stock Platform/Components Division, ALSTOM Transport Austria GmbH, Vienna, Austria

Received: October 07, 2021; Accepted: November 24, 2021

Abstract: The use of induction machine spatial saliencies for sensorless vector control in the proximity of zero electrical frequency has been extensively researched over the last few decades. A robust technique to extract machine saliencies is called voltage step excitation, and it computes a saliency phasor out of phase current derivatives resulting from specific voltage steps generated by the inverter switching. Within the saliency phasor, all machine saliencies appear superposed. For some machine constructions, multiple saliencies are present, containing information about the spatial, magnetic and geometric state of the machine. Due to its direct relation with the rotor angle and its high accuracy, rotor slotting saliency is often chosen as the sensorless control signal. In order to exclusively access rotor slotting, saliency separation needs to be carried out, with the goal of eliminating all non-control saliencies from the saliency phasor. In this research, feedforward harmonic compensation based on look-up tables (LUTs) is chosen. The idea is to estimate each saliency in relation to amplitude and phase shift once, store such information in a torque-dependent LUT and use it for feedforward compensation. Yet, several saliencies are linked to the rotor position and, thus, the stored phase shift in the LUT is fixed to a defined rotor position at which the saliency estimation was performed. For the feedforward compensation to work during each sensorless start-up, an initial rotor slot detection must be carried out. This paper presents a technique to estimate initial rotor angle based only on the inherent characteristics of the induction machine multi-saliencies and an iterative feedforward compensation process that requires no extra resources and only a few PWM (Pulse Width Modulation) periods to achieve initial slot rotor angle. Experimental results measured at two different test benches prove the high accuracy of the method.

Keywords: Induction machines • harmonic compensation • rotor slotting saliency • sensorless control

1. Introduction

Some induction motor designs present multiple spatial saliencies that periodically modify the air-gap flux following a sinusoidal shape. Since saliencies contain information about rotor position or flux, accurate extraction of saliencies permits elimination of position sensor, which is commonly required for vector control schemes. The extraction and use of induction machine spatial saliencies for sensorless vector control in the proximity of zero electrical frequency have been deeply investigated over the last few decades. This is because, in the very low speed region, fundamental wave models and observers deteriorate their performance due to non-linear inverter switching properties and model parameter uncertainties (Holtz and Pan, 2002). A typical classification of saliency extraction techniques divides them into high-frequency injection methods (e.g. Chen et al., 2015; Degner and Lorenz, 1997; Diaz-Reigosa et al., 2013; Jang et al., 2004; Lin and Zhu, 2015; Teske et al. 2000; Yoon and Sul, 2014;) and voltage step excitation (e.g. Gao et al., 2007; Makys et al., 2006; Rodriguez-Montero et al., 2021). The first group injects a high-frequency signal, superposed to the fundamental reference voltage, and extracts motor saliencies from the measured phase currents after several filtering stages. Due to the filtering issues at very low frequencies and the creation of fictitious saliencies caused by inverter nonlinearities, some researches opt for voltage step excitation strategies instead.

* Email: eduardo.montero@tuwien.ac.at

According to the stator voltage equation, the stator current slopes that result from applying a voltage step through the inverter switching are proportional to the transient leakage inductance. Motor saliencies are reflected within the transient leakage inductance. Consequently, transient leakage inductance can be defined as the sum of a constant term, which would exist on its own if the induction machine was perfectly symmetrical, plus multiple saliency-modulated terms, which account for all machine saliencies. Yet, stator current slopes relate to not only transient leakage inductance but also two main distortions, namely stator resistance voltage drop and back electromotive force (EMF).

In order to eliminate stator resistance voltage drop and back EMF, specific combinations of current slopes resulting after certain voltage steps are required. Typically, a subtraction of current slopes resulting from the excitation of two inverter states (out of which one must be active) is performed to successfully eliminate such distortions. In this work, one active excitation is carried out, characterised by the excitation of the machine with a single active inverter state and an inactive state, which rotate together with the fundamental voltage (Rodriguez-Montero et al., 2019). A vector sum of the current slope difference is performed, which yields a saliency-offset phasor. As in the transient leakage inductance, saliency-offset vector (SOV) is composed of a constant term, coming from symmetrical machine, and a saliency-modulated term, where all saliencies are superposed. After offset compensation, all that remains is a saliency vector (SV), where all saliencies appear superposed.

For some designs, induction machines show three dominant saliencies, namely saturation, slotting and intermodulation (Wolbank and Metwally, 2008). The saturation effect of the fundamental wave flux modifies the leakage path permeance, thus modulating transient leakage inductance. This saliency is the most common and rotates with twice the electrical frequency. The slotting saliency is created by the air-gap length variation due to the N_R rotor slots, and thus completes N_R periods within a mechanical revolution. The intermodulation saliency is created by the interaction of the slotting and saturation saliencies, and thus its associated frequency, which is proportional to both mechanical and electrical frequencies.

As the slotting is directly bound to the rotor position, its often chosen as sensorless control signal. For exclusively extracting slotting from the total SV, saliency separation is required. In general, three methods can be applied: filtering (e.g. Caruana et al., 2003; Chen et al., 2015; Holtz and Pan, 2002;), feedforward compensation (e.g. Rodriguez-Montero et al., 2021; Teske et al., 2001; Wolbank and Metwally, 2008) or a combination of both (Gao et al., 2007; Makys et al., 2006). Within filtering, various methods have been presented in the literature, such as spatial filtering (Holtz and Pan, 2002), synchronous filtering (Gao et al., 2007) or Kalman filter (Caruana et al., 2003). However, they may become unstable in case saliency harmonics have similar frequencies or even overlap (Wolbank and Metwally, 2008). Alternatively, feedforward compensation can overcome the scenario of overlapping saliency frequencies. It relies on a commissioning that estimates the amplitude and phase shift of each non-control saliency phasor and stores it in some sort of torque-dependent memory or Look-Up Table (LUT). Several estimation methods have been proposed to identify saliency information, such as neural networks (Wolbank and Metwally, 2008) or cost function (Fahrner et al., 2018). Saliency information stored in the LUT is later accessed with the estimated torque to eliminate all undesired saliencies from the SV. Additionally, absolute electrical and mechanical angles are required in case electrical-related and mechanical-related saliencies are to be compensated. For the induction machines used in this work, intermodulation and saturation saliencies must be compensated, while slotting serves as a control signal.

Rodriguez-Montero et al. (2021) investigated the concept of saliency separation using feedforward compensation for a multi-saliency induction machine during sensorless start-up. At first instant of the sensorless start-up, an electrical angle is available, whereas there is no knowledge of the rotor slot position, which is needed in order to compensate the intermodulation saliency harmonic in case feedforward saliency compensation is used. In Rodriguez-Montero et al. (2021), a strategy to estimate initial rotor slot angle during sensorless start-up was presented. This paper further investigates the strategy presented in Rodriguez-Montero et al. (2021), which was applied to a single inverter traction motor, and provides additional results as well as new measurements taken on a single-inverter dual 14 kW motor test bench.

2. Saliency Extraction Using One-Active Inverter State Excitation

2.1. Saliencies in induction motors

Figure 1 shows the DC-link inverter-machine system, where the induction machine (IM) is represented by its transient leakage inductance, the stator resistance and back EMF. U denotes the voltage, I the current, R the stator

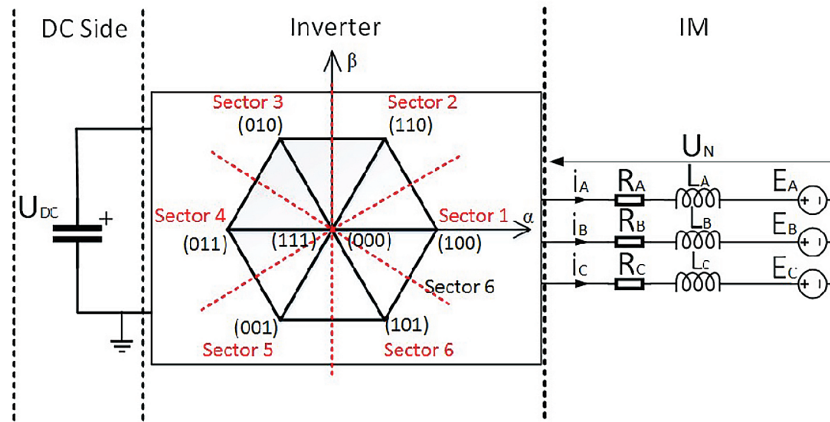


Fig. 1. DC link inverter machine system.

resistance, L the transient leakage inductance, E the phase back EMF, ABC the three phase sub-indices and N an arbitrary phase. Within the inverter, the eight inverter switching states are shown in the alpha-beta plane.

As mentioned before, the geometric and magnetic design of certain induction machines leads to spatial saliencies that periodically modify the air-gap path, thus delivering information about rotor position or flux. Therefore, the transient leakage shown in Figure 1 can be expressed as:

$$L_A = L_0 + \sin(\gamma_m) \quad (1)$$

$$L_B = L_0 + \sin(\gamma_m + 2 \cdot \pi / 3) \quad (2)$$

$$L_C = L_0 + \sin(\gamma_m + 4 \cdot \pi / 3) \quad (3)$$

where the constant term or offset L_0 accounts for the mean value of the inductance, which would exist on its own if there were no spatial asymmetries in the machine. The sinusoid represents the effect of a single spatial asymmetry that rotates with γ_m angle, although there are three main saliencies in induction machines. The saturation saliency always has a significant role, and has been used as a control signal typically in synchronous motors due to its high amplitude, which increases as the machine is loaded. It is produced by the unevenness of the saturation level of the machine lamination. Its frequency is twice the electrical one, and, for this reason, presents a weak angle resolution. The slotting saliency is caused by the slotting of the stator and rotor lamination. Its amplitude can be relevant depending on the machine construction. In terms of frequency, it is directly related to the mechanical frequency and the number of rotor slots. A third saliency is originated by the interaction of saturation and slotting, and it is known as intermodulation. Its amplitude increases with the machine loading. Its frequency is the saturation frequency \pm the slotting frequency.

2.2. Saliency extraction using one-active voltage step excitation

According to the stator voltage equation, under any active inverter switching state, the stator transient leakage inductance, stator resistance and back-EMF can be related to the current derivate as in Eq. (4), U_N taking the values of $\pm 2/3U_{DC}$, $\pm 1/3U_{DC}$ or 0 depending on the phase and switching states (Figure 1).

$$(U_N - R_N \cdot i_N - E_N) \cdot 1 / L_N = di_N / dt \quad (4)$$

As Eqs (1)–(4) show, after a voltage step is applied, current slope calculation on the measured stator currents delivers information about stator transient leakage inductance L_N , defined as a sine wave in Eqs (1)–(3), and also about other line voltage distortions, namely, stator resistance voltage drop and back-EMF. In order to transform saliency term into a phasor, current slopes can be vector combined as in Eq. (5). As reported in the literature (e.g. Makys et al., 2006), the subtraction of two phase currents slopes, among which at least one results from an active

state excitation, suffices to eliminate stator resistance voltage drop and back-EMF; and thus, phase current slope difference exclusively relates to the stator transient leakage inductance and DC-link voltage.

$$\frac{di_{100}}{dt} - \frac{di_{111}}{dt} = \frac{di_{A,100}}{dt} - \frac{di_{A,111}}{dt} + \left(\frac{di_{B,100}}{dt} - \frac{di_{B,111}}{dt} \right) \cdot e^{i \cdot 2 \frac{\pi}{3}} + \left(\frac{di_{C,100}}{dt} - \frac{di_{C,111}}{dt} \right) \cdot e^{i \cdot 4 \frac{\pi}{3}} \quad (5)$$

If the DC voltage is assumed constant, the phase current difference between an active inverter state and an inactive inverter state results in the so-called SOV, as shown in Table 1; this is due to the application of Eqs (1)–(5) to the three machine phases for each active inverter state excitation (Rodriguez-Montero et al., 2019).

In Table 1, ‘cst’ means

$$cst = \left(L_0^2 + \frac{1}{4} \cdot L_m^2 \right) / U_{DC} \quad (6)$$

As presented in Rodriguez-Montero et al. (2019), the voltage step excitation used in this work is embedded in the SVPWM sequence. The actual longest active state is extended to a minimum defined time in order to guarantee a reliable current slope determination. As the fundamental voltage rotates, the SOV varies depending on the actual inverter sector, as defined in Figure 1. In Rodriguez-Montero et al. (2019), signal processing was proposed to deal with the sector-dependent nonlinear offset and phase shift difference. The offset was identified during the commissioning for each torque level and eliminated from the SOV via feedforward compensation. After offset elimination, SV is obtained. In this work, offset is estimated and feedforward compensated using the same scheme as in Rodriguez-Montero et al. (2019).

2.3. Saliency separation

In many induction machines, multiple saliencies are present. They appear superposed in the SV. It is then the task of the saliency separation scheme to isolate a single saliency from which either rotor flux angle or rotor position will

Table 1. SOV using one-active excitation

| Inverter sector | Slope combination | SOV |
|-----------------|---|---|
| S1 | $\frac{di_{100}}{dt} - \frac{di_{111}}{dt}$ | $\frac{L_{0,S1} - \frac{1}{2} \cdot L_m \cdot e^{i \cdot \gamma_m}}{cst}$ |
| S2 | $\frac{di_{\bar{u}}}{dt} - \frac{di_{\bar{u}}}{dt}$ | $\frac{-L_{0,S2} \cdot e^{i \cdot 4 \frac{\pi}{3}} - \frac{1}{2} \cdot L_m \cdot e^{i \left(\gamma_m + 2 \cdot \frac{\pi}{3} + \pi \right)}}{cst}$ |
| S3 | $\frac{di_{010}}{dt} - \frac{di_{111}}{dt}$ | $\frac{L_{0,S3} \cdot e^{i \cdot 2 \frac{\pi}{3}} - \frac{1}{2} \cdot L_m \cdot e^{i \left(\gamma_m + 4 \cdot \frac{\pi}{3} \right)}}{cst}$ |
| S4 | $\frac{di_{011}}{dt} - \frac{di_{111}}{dt}$ | $\frac{-L_{0,S4} - \frac{1}{2} \cdot L_m \cdot e^{i \left(\gamma_m + \pi \right)}}{cst}$ |
| S5 | $\frac{di_{001}}{dt} - \frac{di_{111}}{dt}$ | $\frac{L_{0,S5} \cdot e^{i \cdot 4 \frac{\pi}{3}} - \frac{1}{2} \cdot L_m \cdot e^{i \left(\gamma_m + 2 \cdot \frac{\pi}{3} \right)}}{cst}$ |
| S6 | $\frac{di_{101}}{dt} - \frac{di_{111}}{dt}$ | $\frac{-L_{0,S6} \cdot e^{i \cdot 2 \frac{\pi}{3}} - \frac{1}{2} \cdot L_m \cdot e^{i \left(\gamma_m + 4 \cdot \frac{\pi}{3} + \pi \right)}}{cst}$ |

SOV, saliency-offset vector.

be extracted. In this work, slotting is chosen as control signal, and thus saturation and intermodulation are to be compensated. As stated in the introduction, for exclusively extracting slotting from the total SV, various methods can be applied, and the present work focuses on feedforward compensation. It is based on the individual identification of all saliency harmonics, approximated as a phasor with A amplitude and θ phase shift, as a function of the torque. It stores saliency information in a LUT that is later accessed during online operation. The compensation LUT receives the estimated torque and the saliency angle (e.g. twice the electrical angle for the saturation saliency), and outputs all estimated saliencies amplitude and phase, which are then used for feedforward compensation from the SV, leading exclusively to the rotor slotting saliency.

The estimation of the saliency amplitude and phase shift has been done in many ways, such as neural networks (Wolbank and Metwally, 2008), filters above a threshold speed (Makys et al., 2006) or cost function (Fahrner et al., 2018). In this work, saliencies are identified by means of a cost function for several torque points. The cost function minimises the absolute error between the SV and the sought saliency. In Eqs (7) and (8), cost function is applied to identify the saturation 'sat' and intermodulation 'inter' saliencies.

$$(A_{sat}, \theta_{0,sat}) = \min \left[\text{mean} \left(\text{abs} \left(SV - A_{sat} \cdot e^{i(2\theta_e - \theta_{0,sat})} \right) \right) \right] \quad (7)$$

$$(A_{inter}, \theta_{0,inter}) = \min \left[\text{mean} \left(\text{abs} \left(SV - A_{inter} \cdot e^{i(-N_R \cdot \theta_m - 2\theta_e - \theta_{0,inter})} \right) \right) \right] \quad (8)$$

where θ_e is electrical angle and θ_m is mechanical angle.

2.4. Current slope estimation

In order to accurately estimate current response, this work employs a least-square linear regression. It delivers very precise estimations. This is very convenient since, at the beginning of the pulse, high frequency current oscillation occurs, and they take a finite time to fade away. More information can be found in Landsmann et al. (2013).

2.5. Indirect field oriented control (FOC)

FOC is usually employed in high performance dynamic drives. It establishes a rotor-flux-fixed x-y frame, where the x-axis points to the rotor flux and y-axis is 90° shifted.

For acquiring the rotor flux phasor, rotor flux equation is employed, which relies on stator current and rotor position as well as machine parameters. In rotor-fixed coordinates, rotor flux becomes as in Eq. (9):

$$d\Phi_R / dt = R_R / L_m \cdot (-\Phi_R + L_m \cdot i_s) \quad (9)$$

where Φ_R is rotor flux, R_R is rotor resistance, i_s is stator current and L_m is magnetising inductance.

By controlling the x and y current components, rotor flux Φ_R and torque T can be indirectly controlled, as indicated in Eqs (10) and (11):

$$|\Phi_R| = L_m \cdot i_x \quad (10)$$

$$T = i_y \cdot |\Phi_R| \quad (11)$$

2.6. Flowchart of the drive

Figure 2 shows the general signal processing and the proposed strategy for detecting the initial slot angle (θ_0) needed. i_x^* and i_y^* are the current commands in rotor flux oriented coordinates.

As Figure 2 shows, indirect FOC is performed by controlling the x-y current components. The flux angle that defines the x-y frame is computed as in Eq. (9). The current is controlled using two PIs, one for each axis, whose output is transformed using the park transformation into the stator frame. The motor is then excited according to the strategy presented in Rodriguez-Montero et al. (2019).

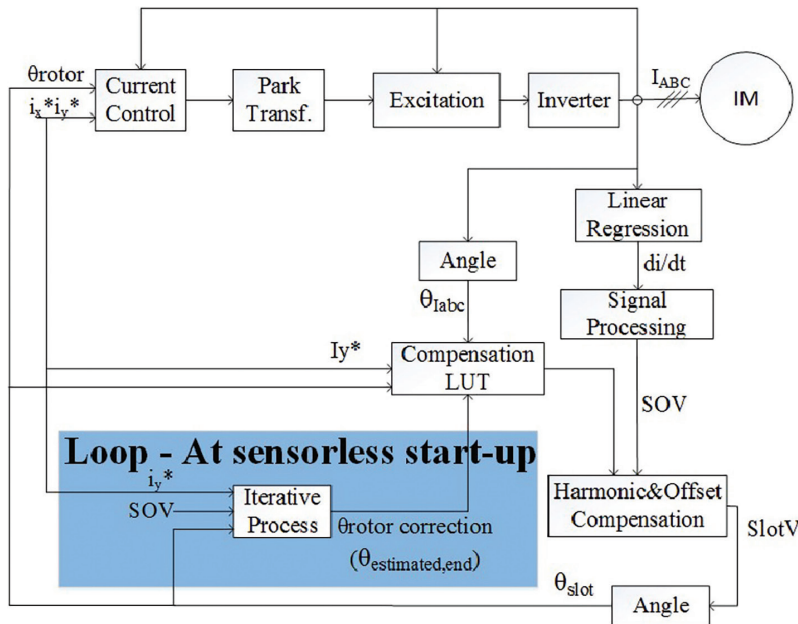


Fig. 2. FOC scheme with integrated slotting extraction and initial rotor slot angle detection. FOC, field oriented control; SOV, saliency-offset vector.

Furthermore, the current slope of the measured stator current is calculated using a linear regression. The calculated current slopes are processed as explained earlier in this section, resulting in the SOV. After feedforward compensating signal offset and non-control saliencies using the compensation LUT, only slotting saliency remains, which is used as position signal for the rotor flux acquisition required in Eq. (9). The initial rotor detection scheme marked in Figure 2 in blue will be explained in following section.

3. Sensorless start-up strategy

At the first instant of the sensorless start-up, there is no knowledge about the rotor slot position. This is because without the position encoder, the sensorless drive has no knowledge of the actual relative position of the rotor slot. However, this information is necessary for the saliency separation technique to work, as it requires a mechanical angle that is fixed to a defined slot position as input to the LUT. This is depicted in Figure 3, where the modulated transient inductance sees its minimum at the centre of each rotor slot (black trace).

Figure 3 shows an example of an actual slotting saliency ($L_{m,actual}$ black trace), having an arbitrary phase shift of $\theta_{slot,actual}$. Since there is no knowledge about the rotor position during encoderless start-up, a sensorless estimated saliency is defined as in Figure 3 (red dotted trace), where the phase shift is set arbitrarily to zero. In order to calculate the phase shift of the slotting signal, a strategy is required for the mechanical sensorless angle (equal to zero at start-up) to converge to the actual rotor slot angle. In Rodriguez-Montero et al. (2021), a method was presented to estimate the slot angle ($\theta_{slot,actual}$ depicted in Figure 3) needed for the feedforward intermodulation compensation based on LUT. The output of this method is the angle $\theta_{estimated,end}$ based on an iterative process that makes the sensorless estimated angle $\theta_{estimated,end}$ converge to the actual angle $\theta_{slot,actual}$.

As defined in Figure 3, 360 Slot° are equivalent to one revolution of the rotor slotting signal.

3.1. Initial rotor angle detection: graphical explanation

A graphical explanation of the process is shown in Figure 4, where three harmonics are involved and the slotting is selected as the control signal. Thus, saturation and intermodulation are feedforward compensated via compensation LUT. It is worth noting that the actual slotting vector (SlotV) would come from an encoder that is never used except for comparison reasons.

By looking at Figure 4a, we observe that the SV is plotted together with the three harmonics that are forming it. These are saturation (red), slotting (pink) and intermodulation (blue). Due to the known electrical angle, the

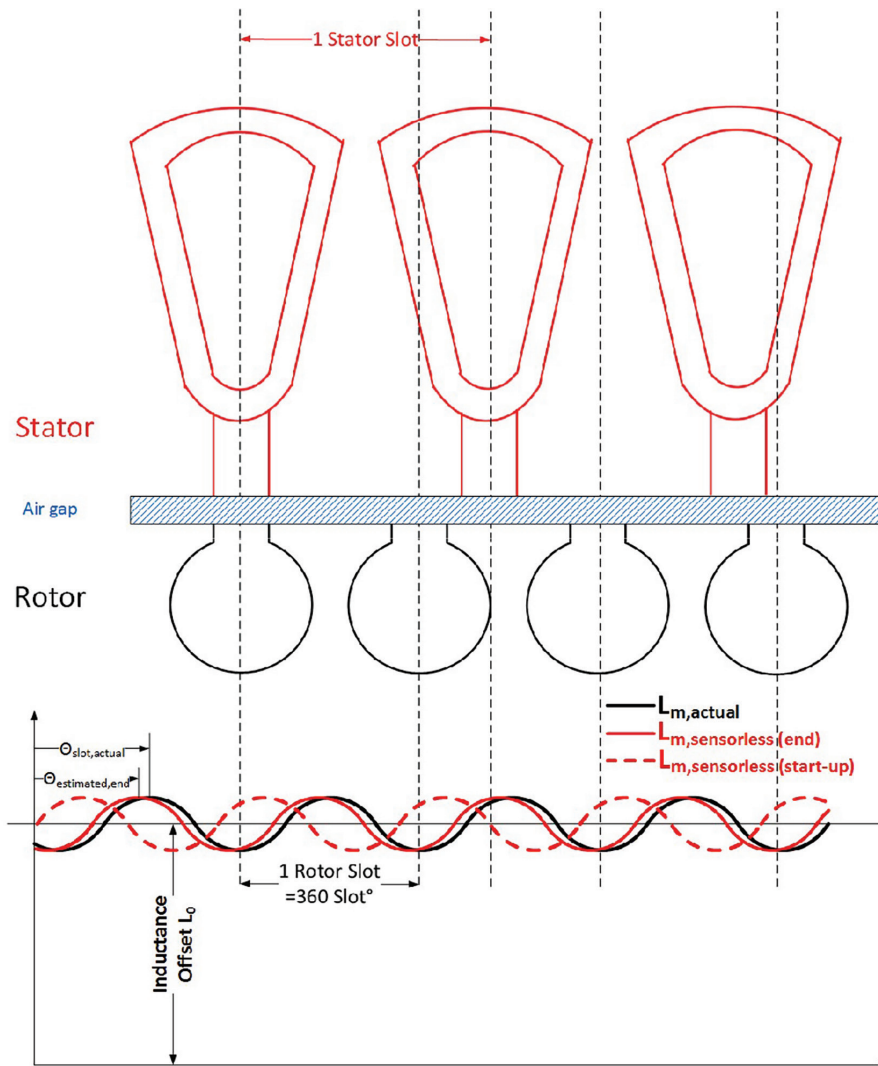


Fig. 3. Example of slotting saliency with and without encoder at start-up.

saturation can be accurately compensated, and will be no more relevant for the initial slotting angle estimation. That is why in Figure 4b, the saturation does not appear anymore, as it is assumed to be fully compensated. Besides, given that the sensorless mechanical angle is unknown at first, it is forced to zero. This leads to an angle error between the sensorless estimated slotting and actual slotting at start-up of 110° (in Figure 4, $\theta_{0,start-up}$), which leads to an error at the intermodulation estimated angle (-40° estimated at start-up instead of -150° actual).

With the start-up estimated slotting and intermodulation angle, the iterative process begins. In Figure 4b, a compensation of the intermodulation is performed with the start-up estimated value. This ends up in a new slotting estimated angle $\theta_{slot,estimated}$, which still contains a relevant error ($\theta_{0,1}$). Slotting error θ_0 is therefore defined as the difference between the actual slotting angle and the estimated one:

$$\theta_0 = (\theta_{slot,estimated} - \theta_{slot,actual}) \tag{12}$$

where $\theta_{slot,actual}$ is the actual phase shift of the slotting saliency, only used for explanatory reasons here.

During the next iteration (Figure 4c), a compensation of the intermodulation is performed with the estimated value of the intermodulation angle of previous iteration (iteration 1). This leads to a new slotting estimated angle, which still contains some error ($\theta_{0,2}$).

The third iteration is carried out in the same way as iterations 1 and 2. The slotting error is negligible at the end of this iteration, meaning that the method converged to the expected value. As can be seen in Figure 4d, a small mismatch may remain between the actual and estimated intermodulation angle ($\theta_{inter_error_3}$), since the saliencies amplitude and angle play an important role in the convergence speed and characteristics of the method.

This process is repeated until the slotting estimated angle stabilises, or depending on noise/precision requirements.

3.2. Initial rotor angle detection: signal flowchart

The signal flowchart of the sensorless initial rotor position estimation is shown in Figure 5.

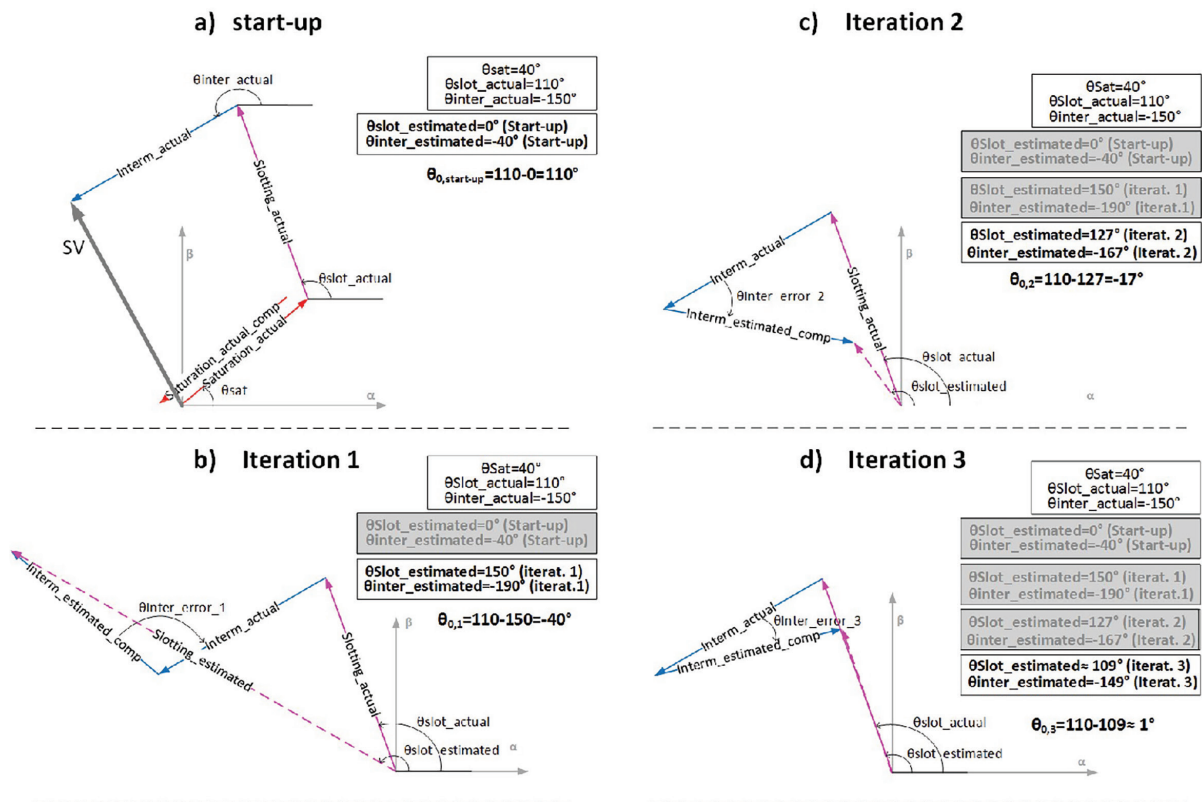


Fig. 4. Graphical explanation of initial rotor angle detection method during (a) start-up, (b) iteration 1, (c) iteration 2 (d) iteration 3.

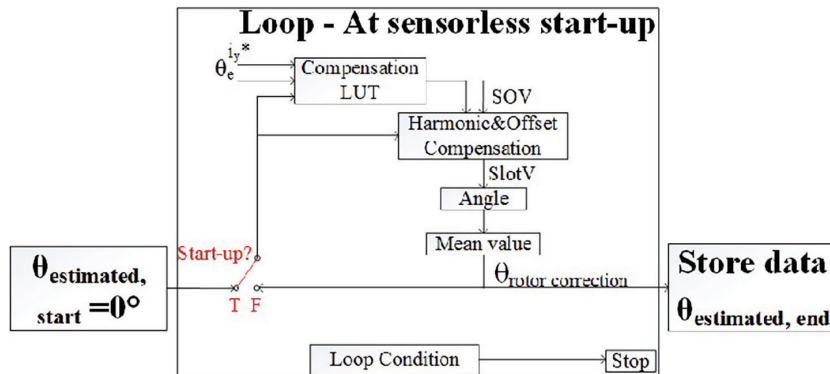


Fig. 5. Method for sensorless initial rotor slot detection. LUT, Look-Up Table; SOV, saliency-offset vector; SlotV, slotting vector.

As shown in Figure 5, the proposed angle estimation is implemented in a loop. During the first execution, the rotor slot angle is unknown. Therefore, $\theta_{\text{estimated,start}}$ is forced to zero and sent to the compensation block, which obtains a new estimated SlotV, a new correction angle and therefore a new estimation angle, $\theta_{\text{estimated}}$ [Eq. (12)]. For increased performance, a mean value of 10 consecutive angles is performed. During subsequent executions, $\theta_{\text{estimated}}$ instead of $\theta_{\text{estimated,start}}$ is used. The last iteration correction angle $\theta_{\text{estimated,end}}$ is the angle that is used for the sensorless operation.

4. Test Bench Description

4.1. Test bench 1

The strategy presented in this paper is applied to a high power motor used in railway applications using one-active angular voltage step excitation. During speed control, the motor is controlled at 5 rpm. Indirect FOC is carried out. The power of the motor is in the range of several hundred kW. The rotor is unskewed. The switching frequency is set to 1 kHz. The minimum pulse duration for di/dt estimation is set to 80 μs . Current slope is estimated using least square linear regression with current being measured at 2 MS/s.

4.2. Test bench 2

In addition, the strategy presented in this paper is applied to a second test stand. It consists of two unskewed 14 kW induction motors connected in parallel and fed by a single inverter. As in the previous test bench, switching frequency is set to 1 kHz and the minimum pulse duration for di/dt estimation is set to 80 μs . Current slope is estimated using least square linear regression with current being measured at 2 MS/s. A belt drive is implemented to ensure synchronous rotation of both motors.

5. Experimental Results – Test Bench 1

5.1. Full sensorless operation

Figure 6 shows the initial rotor slot angle detection at an initial slot position of 279 Slot°, measured by an encoder used only for comparison reasons. The experimental test is divided in a few intervals, defined in Table 2:

At instant 0 \rightarrow 1, the rotor is magnetised for a specific time to ensure constant rated rotor flux. At beginning of interval 1 \rightarrow 2, angle estimation takes place, where three iterations are performed. The estimated angle takes the value of 0°, 242.6 Slot°, 269.2 Slot° and 284.6 Slot°. During interval 2 \rightarrow 3, speed control is performed.

As seen in Figure 6, the slotting signal (left plot, row 2) does not contain any other saliency superimposed during the speed controlled interval. As the initial angle correction was performed, the intermodulation, as well as saturation, was compensated from the SV (right, row 1) without position sensor at any time. It can be seen that at interval 1–2, a few iterations for angle correction occur. This leads to the noticeable change in the slotting signal real and imaginary values (row 2, left).

Regarding slotting angle estimation, it takes the value of 0 Slot° at start-up, 242.6 Slot° after the first iteration, 269.2 Slot° after the second iteration and 284.6 Slot° at the end iteration. For the given saliency amplitudes, four iterations are always enough for the method to converge, as the intermodulation amplitude is never bigger than the slotting amplitude.

The mechanical angle deviation is always kept in the range of $\pm 2^\circ$ (mechanical degrees), which also proves the accuracy of the sensorless operation using the proposed angle correction.

5.2. Accuracy of initial rotor slot angle detection

In order to analyse the accuracy of the angle estimation, a second experimental test is performed. It consists of eight different measurements. The sensorless slot angle at the end of estimation process is calculated for several initial slot positions, in the range from 0 Slot° to 360 Slot°, in order to prove that the method can converge to a final value independent of the starting slot position. The strategy proposed in this paper is carried out in eight separated experiments at (almost) equally distanced rotor slot position (in Slot°). The end estimated slot angle is compared with the encoder angle, which ultimately defines the capability of the sensorless method in estimating the initial rotor position. This is shown in Figure 7.

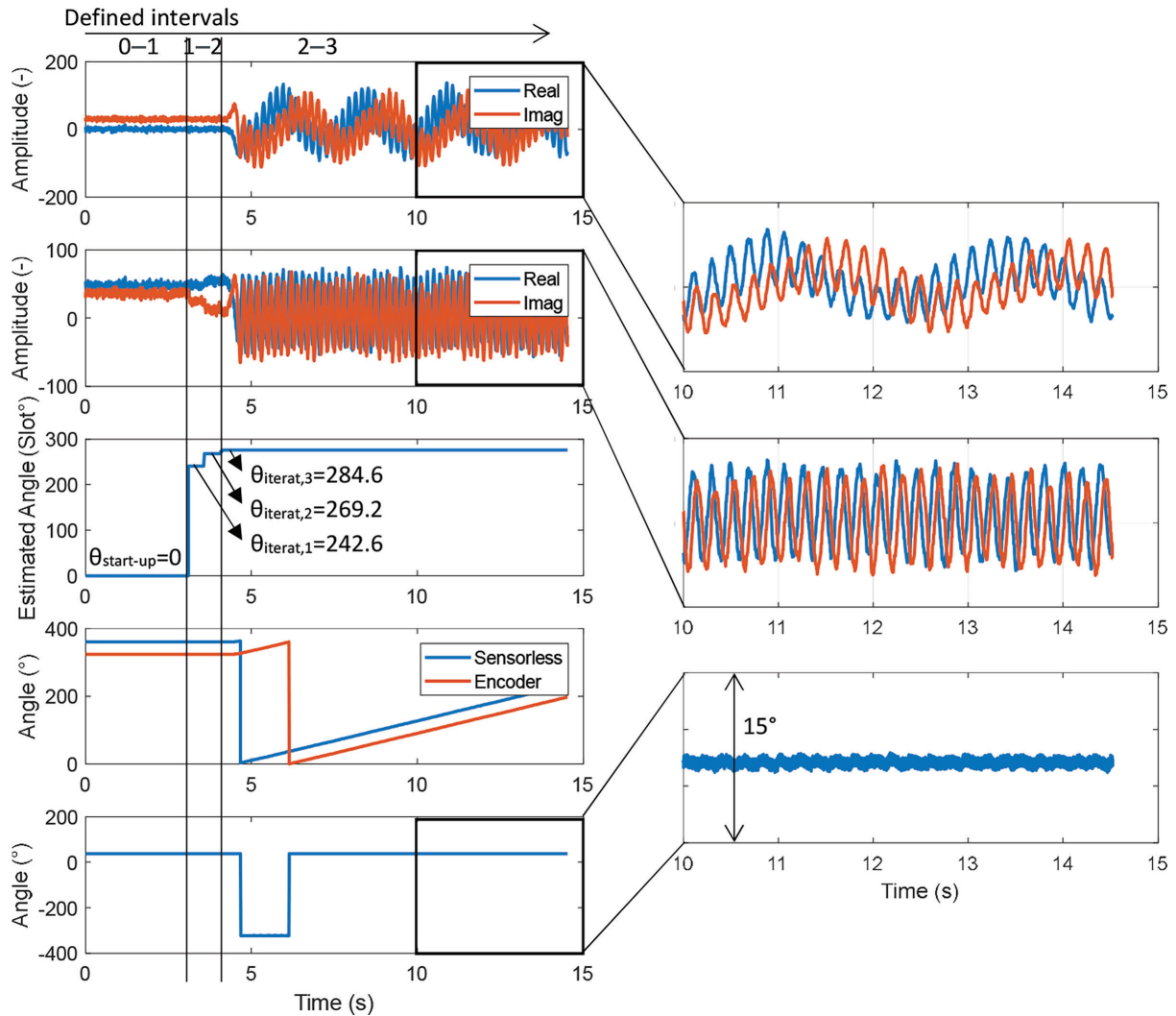


Fig. 6. Initial slot angle estimation at 279 Slot°. Row 1: SV. Row 2: SlotV. Row 3: estimated slot angle ($\theta_{\text{slot_estimated}}$). Row 4: sensorless mechanical angle and encoder. Row 5: mechanical angle deviation. SlotV, slotting vector; SV, saliency vector.

Table 2. Intervals defined for sensorless operation

| Interval 0 → 1 | Interval 1 → 2 | Interval 2 → 3 |
|----------------|------------------|----------------|
| Magnetisation | Angle Estimation | Speed Control |

The slot angle estimation error is calculated as in Eq. (12).

6. Experimental Results – Test Bench 2

An experiment similar to that of Section 5.1 is applied to the dual motor test bench in order to prove the applicability under different test motors and drive configurations. As in Section 5.1, the intervals of this experiment are the same: magnetisation, rotor slot angle estimation and speed control. Figure 8 shows the results for both motors (left: M1, right: M2).

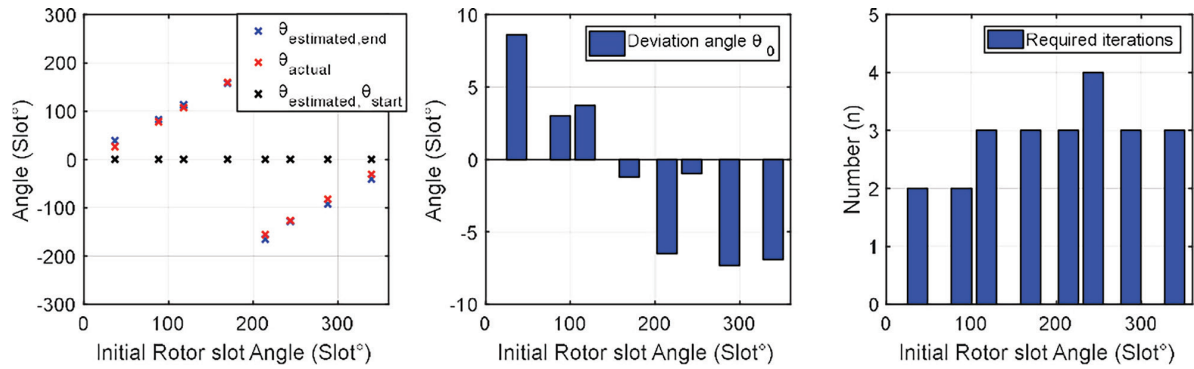


Fig. 7. Angle estimated and final angle estimation error within one rotor slot. Column 1: sensorless estimated end angle, sensorless estimated start-up angle and actual (from encoder) angle. Column 2: Deviation angle as in Eq. (12). Column 3: Number of iterations.

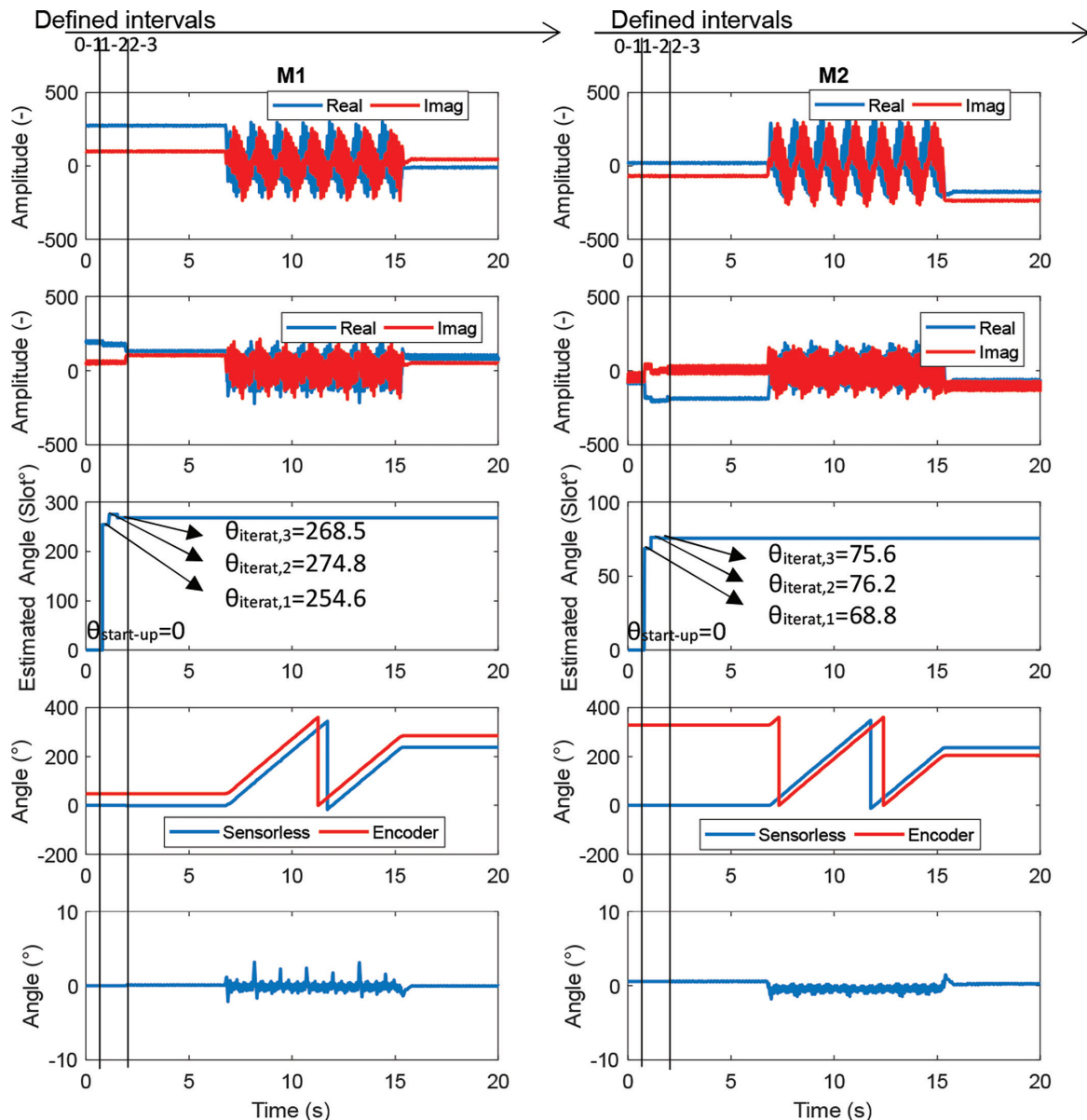


Fig. 8. Initial slot angle estimation at 259 Slot (M1) and 73 Slot (M2). Row 1:SV. Row 2: SlotV. Row 3: estimated slot angle ($\theta_{slot_estimated}$). Row 4: sensorless mechanical angle and encoder. Row 5: mechanical angle deviation. SlotV, slotting vector; SV, saliency vector.

As observed in Figure 8, the SV (row 1) is processed to form a SlotV (row 2) by feedforward eliminating saturation and intermodulation saliencies, separately for each motor. Note that a small fraction of other harmonics apart from the slotting remain in the SlotV, although they do not impede sensorless rotor extraction as the slotting saliency dominates. After initial slot angle is estimated, speed control is performed. During speed control, both motors rotate synchronously at 10 rpm until $t = 15$ s. From that point, speed is set to zero to show performance at mechanical standstill.

7. Conclusions

Some motors exhibit multiple saliencies. They can be accessed by voltage steps, evaluating resulting current slopes and forming a SV, which is a vector where all saliencies are superposed. The extraction of rotor slotting for sensorless control is often done by the feedforward compensation of the non-control saliencies from the total SV. This compensation scheme requires each saliency to be identified in relation to its amplitude and phase shift fixed to the revolving angle. Yet, some saliencies are linked to the rotor angle, such as intermodulation and slotting. Therefore, during sensorless start-up, as there is no knowledge on initial rotor position, an initial rotor angle estimation must be performed, so that the feedforward compensation scheme can work successfully.

The present study has investigated the initial rotor angle estimation strategy proposed in Rodriguez-Montero et al. (2021), and applied the concept to a dual-motor single inverter drive. The presented experimental results have proved the accuracy of the initial rotor angle detection scheme, which requires no additional resources and takes only a few modulation periods to converge. The method has been applied to induction motors that possess three dominant saliencies: saturation, intermodulation and slotting. Further, saliency feedforward compensation was successfully achieved with the use of the proposed initial rotor angle detection. Thus, slotting-based rotor position acquisition during sensorless speed control was highly accurate, as proved by the very low encoder to sensorless angle deviation ($\pm 2^\circ$) obtained during experimental test.

Acknowledgements

This research is supported by Austrian Research Promotion Agency (FFG) under the Bridge-program, grant No. 858502. The authors want to thank ALSTOM (Bombardier Transportation joined Alstom Group in 2021), especially Mr. H. Mannsbarth (head of Components-Bogies/Drives department in global Rolling Stock Platform/Components division) for his generous support, research/development funding and project supervision. Furthermore, the authors want to thank colleagues from ALSTOM group (Mr. Sorg, Mr. Cepak, Mr. Harasleben, Mr. Ganster and Mr. E. Moser), as well as Prof. Dr. H. Ertl (TU-Wien), for all their feedback. The authors are highly indebted to LEM Company (especially Mr. A. Hürlimann/Chair of Board of Directors, Dr. W. Teppan and Mr. J. Burk) for cooperation and generous support.

*This article was selected for publication in this journal after the IEEE-PEMC 2020 conference.

References

- Caruana, C., Asher, G. M., Bradley, K. J. and Woolfson M. S. (2003). Flux Position Estimation in Cage Induction Machines Using Synchronous Injection and Kalman Filtering. *IEEE Transactions on Industry Applications*, 39(5), pp. 1372–1378.
- Chen, Z., Zhang, Z., Kennel, R. and Luo, G. (2015). Hybrid sensorless control for SPMSM with multiple saliencies. In: *41st Annual Conference of the IEEE Industrial Electronics Society*, Yokohama, 9–12 November 2015.
- Degner, M. W. and Lorenz, R. D (1997). Using Multiple Saliencies for the Estimation of Flux, Position, and Velocity in AC Machines. In: *Proceedings of IEEE IAS Annual Meeting*, New Orleans, 5–9 October 1997.
- Diaz-Reigosa, D., Briz, F., Blanco-Charro, C, Di-Gioia, A., Garcia, P. and Guerrero, J. M. (2013). Sensorless control of doubly fed induction generators based on rotor high-frequency signal injection. *IEEE Transactions on Industry Applications*, 49(6), pp. 2593–2601.

- Fahrner, W., Vogelsberger, M. A. and Wolbank, T. (2018). A new technique to identify induction machine rotor parameters during dynamic operation and low speed. In: *IEEE 18th International Power Electronics and Motion Control Conference*, Budapest, 26–30 August 2018.
- Gao, Q., Asher, G. M., Sumner, M. and Makys, P. (2007). Position Estimation of AC Machines over a Wide Frequency Range Based on Space Vector PWM Excitation. *IEEE Transactions on Industry Application*, 43(4), pp. 1001–1011.
- Holtz, J. and Pan. H. (2002). Elimination of saturation effects in sensorless position controlled induction motors. In: *Proceedings of IEEE Industry Applications Annual Meeting*, Pittsburg, 13–18 October.
- Jang, J.-H., Ha, J.-I., Ohto, M., Ide, K. and Sul S. K. (2004). Analysis of Permanent-Magnet Machine for Sensorless Control Based on Highfrequency Signal Injection. *IEEE Transactions on Industry Applications*, 40(6), pp. 1595–1604.
- Landsmann, P., Paulus, D. and Kennel, R. (2013). Silent and parameter independent hybrid sensorless control for SPMSM based on current oversampling. In: *IEEE International Symposium on Sensorless Control for Electrical Drives and Predictive Control of Electrical Drives and Power Electronics*, Munich, 17–19 October 2013.
- Lin, T. C. and Zhu, Z. Q. (2015). Sensorless Operation Capability of Surfacemounted Permanent-Magnet Machine based on High-Frequency Signal Injection Methods. *IEEE Transactions on Industry Applications*, 51(3), pp. 2161–2171.
- Makyš, P., Asher, G. M., Sumner, M., Gao, Q. and Vittek. J. (2006). A Low Memory Disturbance Elimination Method for Sensorless Control of Induction Motor Drive using Test Vector Injection. In: *Proceedings of the Annual Conference of the IEEE Industrial Electronics Society*, Paris, 6–1 November 2006.
- Rodriguez-Montero, E., Vogelsberger, M. A. and Wolbank, T. (2019). Robust Signal Offset Identification for Sensorless Control of Induction Machines at Rated Load using One-Active Modulating Pulse Excitation. In: *IEEE Energy Conversion Congress and Expo*, Baltimore, 29 September–3 October 2019.
- Rodriguez-Montero, E., Vogelsberger, M. A. and Wolbank, T. (2021). Sensorless identification of the initial rotor slot position using one active inverter state excitation in induction machines. In: *Proceedings of the 19th International Power Electronics and Motion Control Conference PEMC*, Gliwice, 25–29 April 2021.
- Teske, N., Asher, G., Bradley, K. and Sumner, M. (2000). Sensorless position estimation for symmetric cage induction motor under loaded conditions. In: *Conference Record of the 2000 IEEE Industry Applications Conference*, Rome, 8–12 October 2000.
- Teske, N., Asher, G., Bradley, K. and Summer, M. (2001). Analysis and suppression of inverter clamping saliency in sensorless position controlled induction machine drives. In: *Conference Record of the 2001 IEEE Industry Applications Conference*, Chicago, 30 September–3 October 2001.
- Wolbank, T. M. and Metwally, M. K. (2008). Saliency tracking-based sensorless control of induction machines using artificial neural networks. In: *12th International Middle-East Power System Conference*, Aswan, 12–15 March 2008.
- Yoon, Y.-D. and Sul, S.-K. (2014). Sensorless Control for Induction Machines Based on Square-Wave Voltage Injection. *IEEE Transactions on Power Electronics*, 29(7), pp. 3637–3645.